The information efficacy of a synapse

Michael London[1], Adi Schreibman[2], Michael Häusser[3], Matthew E. Larkum[4] and Idan Segev[1]

[1] *Department of Neurobiology Institute of Life Sciences and Center for Neural Computation, Hebrew University, Jerusalem 91904, Israel.*

[2] *Department of Computer Science, Hebrew University, Jerusalem 91904, Israel.*

[3] *Department of Physiology, University College London, Gower Street, London WC1E 6BT, UK.*

[4] *Abteilung Zellphysiologie, Max-Planck-Institut für medizinische Forschung, Jahnstraße 29,D-69120 Heidelberg, Germany.*

Correspondence and requests for materials should be addressed to I.S. (idan@lobster.ls.huji.ac.il)

We provide a functional measure, the synaptic information efficacy (SIE), to assess the impact of synaptic input on spike output. SIE is the mutual information shared by the presynaptic input and postsynaptic output spike trains. To estimate SIE we used a method based on compression algorithms. This method detects the effect of a single synaptic input on the postsynaptic spike output in the presence of massive background synaptic activity in neuron models of progressively increasing realism. SIE increased with increases either in time locking between the input synapse activity and the output spike or in the average number of output spikes. SIE depended on the context in which the synapse operates. We also measured SIE experimentally. Systematic exploration of the effect of synaptic and dendritic parameters on the SIE offers a fresh look at the synapse as a communication device and a quantitative measure of how much the dendritic synapse informs the axon.

The word synapsis, later modified to synapse, was coined in 1897 (from the Greek word συναπτω, to clasp) by Lord Sherrington to describe the functional connection between neurons. Sherrington[1] noted that "…each synapse offers an opportunity for a change in the character of nervous impulses, that the impulse as it passes over from the terminal arborescence of an axon into the dendrite of another cell, starts in that dendrite an impulse having characters different from its own." Indeed, it is now common knowledge that the typical chemical synapse transforms the all-or-none spike in the presynaptic axon into a graded response in the dendrites of the postsynaptic neuron, and that the synapse shows activity-dependent modification. We must understand the intricacies of the synapse if we are to comprehend how networks of neurons operate collectively and how memory and learning are embedded in such networks. Over the past 50 years, the synapse has become a focus of intense research, and, as a result, we have become intimately familiar with the fine anatomy, molecular biology and biophysical properties of the synapse.

The understanding of synapses at the functional level is, however, surprisingly limited. Basic questions remain regarding information processing by the synapse, including: What is the appropriate measure for the effect of a synapse? What is the relationship between the biophysical parameters of a synapse (such as the release probability and the amplitude of the postsynaptic potential) and the efficacy of the synapses in the functional sense? Are there plausible learning rules that optimize the effect of a synapse? (See, however, refs 2–5.)

The need to assign a functional meaning to the synapse is reflected in the popular use of the term synaptic efficacy, typically preceded by phrases such as maintenance of, regulation of and redistribution of. In the biophysical realm, synaptic efficacy is typically characterized by parameters associated with specific synaptic mechanisms, such as the number of transmitter quanta released (per spike), the release probability, the peak value (or time integral or rise time) of the postsynaptic potential or the synaptic conductance change[6–7]. If the value of these parameters increases, the synapse should have a stronger impact on the output of the postsynaptic neuron. But which of these parameters is functionally the most relevant? In addition, in experimental explorations of the synaptic effect, researchers typically treat the synapse in isolation, ignoring the fact that *in vivo* the synapse acts in the presence of massive background synaptic activity[8–11]. Should we consider the effect of an isolated synapse, ignoring the context provided by the other active synapses?

A functional link between synaptic parameters and the firing of the postsynaptic neuron is provided by the cross-correlation (CC) measure. Because the shape of the CC is closely related to the time course of the postsynaptic potential[12–13], the question remains: Which of the parameters that characterize the CC is functionally the most relevant, its peak, its rise time or rather its time integral?

A rigorous definition for synaptic efficacy (or synaptic weight) can be found in the field of connectionist theory, in which the synapse is modeled by a single scalar, w_{ij}, that characterizes the strength of the connection between neuron j and neuron i. Within this framework, learning algorithms and memory formation rely on activity-dependent changes in the value of w_{ij}[14–15]. However, in the connectionist framework, neurons are highly simplified elements, and the relationship between the compact description of the synaptic weight, w_{ij}, and the actual biophysical parameters of real synapses is not well defined (but see O. Shriki, *et al., Soc. Neurosci. Abstr.* **24**, 143, 1998).

Fig. 1. Single dendritic synapses, among many other synapses, do matter. (**a**) Layer 5 pyramidal neuron from the cat somatosensory cortex[50] used for the model. 400 excitatory synapses (peak conductance, $G_{syn} = 2$ nS) were uniformly distributed over the dendritic surface (small magenta dots); each synapse was activated randomly 10 times s^{-1}. A further 100 inhibitory synapses were uniformly distributed; each synapse was activated at random, 65 times s^{-1} (cyan dots; see Methods). The dendritic tree and axon were excitable as in ref. 21. (**b**) An extra excitatory input synapse (identical to all other excitatory synapses) was placed at either a proximal or a distal dendritic site (corresponding arrows in **a**). The resultant single somatic EPSPs are plotted in the absence of background synaptic activity. (**c**) Voltage response at the soma when the input synapse was located proximally (red) or distally (blue). In these example traces (800 ms of a 200-s simulation in each case), the difference between the two cases is evident. Except for the re-allocation of the input synapse, all other model parameters were identical for the two simulated cases, including the activation times of the input synapse (marked by vertical bars at bottom) and of the background synapses. (**d**) Histogram of the absolute difference between the somatic voltage traces for the two simulated cases (after removal of spikes), revealing that these differed by >0.5 mV more than 10% of the time. (**e**) The CC between the input spike train and the output spike train for identical simulations, except for the input synapse that was potentiated ($G_{input} = 8$ nS; red, proximal input synapse; blue, distal input synapse).
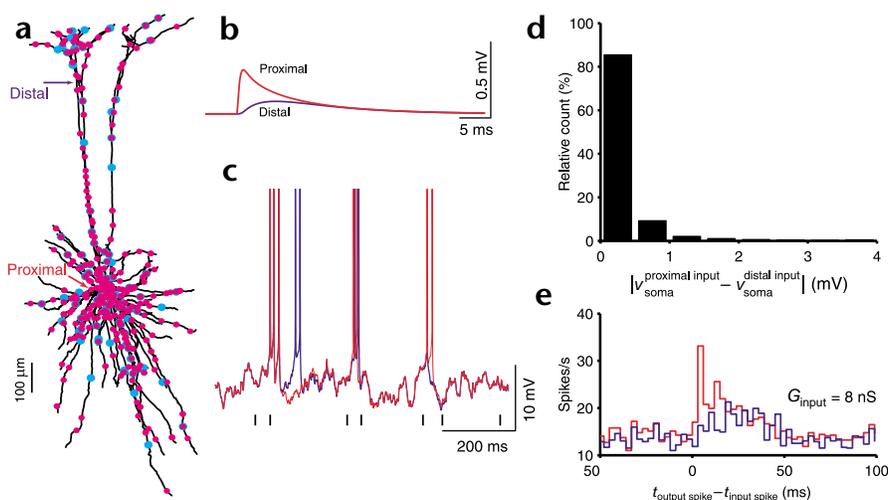
We propose to treat the synapse as a communication device that receives a train of presynaptic spikes and, through a graded analog response, affects the spike train at the postsynaptic neuron. Information theory enables one to quantify the efficacy of the synapse by measuring the mutual information between the input and the output spike trains[4–5,16–18]. This measure is henceforth termed SIE. Utilizing the context-tree weighting compression algorithm[19], we estimated the SIE in the presence of realistic massive background synaptic activity. Consequently, we provide insights into the effect of a variety of synaptic and dendritic parameters, as well as the statistical properties of the background synapses, on the information transmitted by the synapse. Ultimately we would like to know what a single dendritic synapse, among the crowd of many other synapses, tells the postsynaptic axon. This, however, requires knowledge of the neuronal code. Nonetheless, we may ask an intermediate question: how much does the synapse tell the axon?

RESULTS

A single synapse matters for spike output

The dendritic location (proximal versus distal) of even a single excitatory synapse, activated in the presence of massive background synaptic bombardment (**Fig. 1a**), can have a noticeable effect on axonal spike output (**Fig. 1c**). Specifically, some of the output spikes that were elicited in one case disappeared, or were shifted by a few milliseconds, in the other case. Nothing in the very small difference between the two corresponding isolated excitatory postsynaptic potentials (EPSPs) measured at the soma (**Fig. 1b**) explained the marked difference between the two cases (**Fig. 1d**). This nonlinear effect was the result of the threshold for spike firing at the axon, as well as the complex nonlinear interaction between the active soma–axon region and the excitable dendrites[20–24].

Is there a systematic method to quantify the effect of an individual synapse on spike output? This effect depends both on the parameters of the input synapse, in particular the properties of the somatic EPSP[12,25–27], and on the properties of the postsynaptic neuron (cable properties of dendrites, excitability of the

axon) as well as the background synapses. Hence, the effect of a given synapse on spike output should be quantified statistically (as is the CC measure), because it depends on the state of the neuron when the synapse is activated.

The difficulty in quantifying the effect of a synapse using the CC is illustrated in Fig. 1e. Although there was a clear deviation from the baseline for both proximal and distal inputs, it was not clear which parameter of the CC was relevant for quantifying the efficacy of the synapses. In addition, the CC for the proximal input (red) showed two peaks, implying a tendency for spike doublets, whereas no such double peak appeared for the distal input (blue). How should one quantify the difference between these two cases?

Effects of synaptic parameters on SIE

We propose that the mutual information (MI) between the spike train that activates the input synapse and the spike train at the postsynaptic neuron is the natural measure for the efficacy of this synapse. This measure, SIE, functionally links the properties of the synaptic input to the neuron's output.

The concepts of information and entropy are closely linked. Consider the spike train as a sequence of the symbols '0' and '1' (**Fig. 2a**) and the neuron as a generator of these symbols. The entropy rate (in bits s^{-1}) of the output spike train measures the average degree of uncertainty regarding whether the next symbol will be '1' or '0'. The larger the entropy, the less certainty there is. Suppose now that the spike train activating the input synapse is known. If the synapse does affect the output then, on the average, we expect that our uncertainty about the next symbol would decrease. This reduction in uncertainty is quantified by the MI between the input and the output spike trains. Data compression provides another perspective on these quantities (**Fig. 2a**). (For formal definitions of entropy, conditional entropy and MI, see **Supplementary Methods 1** on the supplementary information page of *Nature Neuroscience* online.)

We started with the simplest neuron model, consisting of an isopotential resistance-capacitance (RC) compartment with an
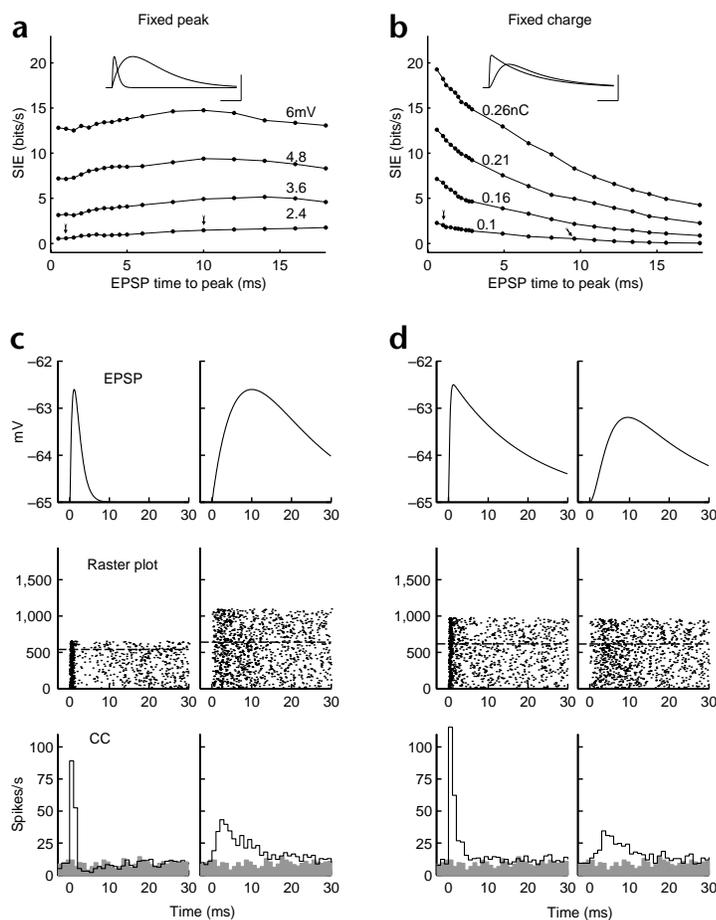
Fig. 2. MI as a measure of synaptic efficacy. (**a**) At left, a model of an isopotential RC compartment with an I&F spike mechanism. The background synaptic input consisted of 400 excitatory synapses and 100 inhibitory synapses activated as described in Methods. We arbitrarily assigned one excitatory synapse to be the input synapse (red) and set the threshold for spike firing at 10 mV above the resting potential. This model produced an average output firing frequency of 10 spikes s^{-1}, with nearly random statistics (coefficient of variation (c.v.) = 0.75–1.1, depending on the strength of the input synapse). At right (blue), a 500-ms stretch of the voltage fluctuation (output). To compute the MI, we transformed all spike trains into strings of '0s' and '1s', using a temporal bin of 3 ms (binned output, blue). An illustrative example for estimating the MI using a compression algorithm is also shown (see Methods for the actual method used). The binned output spike train was compressed using the rules denoted in the green box. This compression resulted in a shorter string of '0s' and '1s' (green). Its length, divided by the total duration of the output, was an estimate of the entropy rate of the output spike train. (The true entropy rate is the limit for a very long string and an ideal compression algorithm.) If the spike train arriving at the input synapse is known, the output spike train can be compressed even further using, for example, the rule described in the lower table with the input 00000001000000000000010000000000000000000000. The length of this short output string (compressed output given input) is the conditional entropy. The MI is the difference between the output entropy and the conditional entropy; it measures how many bits of information were saved in the compressed output spike train by knowing the input. (**b**) The MI (henceforth SIE) between the presynaptic input spike train and the output spike train, as a function of the peak current of the input synapse (filled circles). We also plotted the estimated SIE of one excitatory background synapse (+,SIE$_{control}$), the entropy of the input spike train (dashed line), the entropy of the output spike train (asterisks) and the conditional entropy of the output, given the input spike train (stars). Error bars in the SIE for the input synapse represent 2 s.d., computed over 25 repetitions of the simulation with different seeds. Because of estimation bias for very weak inputs, the estimated SIE could obtain negative values. Because this never exceeded –0.5 bits s^{-1}, no correction was made.

integrate-and-fire (I&F) spike generation mechanism (**Fig. 2a**). In this model, both the input synapse and the background synapses (the noise) were linear current sources. Figure 2b summarizes the results for the case in which the peak current of the input synapse was potentiated. SIE between the input synapse and the output spike train, SIE$_{input\ synapse}$, was a sigmoidal function of the peak synaptic current. For small inputs, the SIE was close to zero and, as expected, it was not markedly different from other background (nonpotentiated) synapses, SIE$_{control}$. With further potentiation, the SIE increased monotonically until it reached saturation. In this regime, the input synapse was so powerful that, when activated, it always triggered an output spike; additional potentiation did not affect further the output and, thus, no information was accrued. Although very strong inputs are physiologically rare (but see ref. 28), the case of a strong temporal correlation among several excitatory synaptic inputs is similar to that of a strong synapse. The saturation of the SIE sets a limit on the number of correlated inputs for maximizing information transmission by this synaptic input[12,29–30] (but see the extension in Fig. 5 for a more realistic, conductance-based spike generation mechanism). For the Poisson input spike train used here, with an average firing rate of $r = 10$ spikes s^{-1} for the excitatory synapses and a sampling bin size of Δt = 3 ms, the entropy was $H = r \times \log_2(e)/(r \times \Delta t) = 10 \times \log_2(e)/(10 \times 0.003) = 65$ bits s^{-1} (**Fig. 2b**; dashed line, input entropy). For any mean firing rate, the input entropy is maximal for spike trains with Poisson statistics, and is zero at the opposite extreme of a regular-input spike train[17].

Figure 2b also depicts the entropy of the output spike train, $H(S_{out})$, as well as the entropy of the output given the input (the conditional entropy, $H(S_{out}|S_{in})$). SIE is the difference between

these two quantities. At low firing rates, assuming nearly Poisson statistics, the probability of a spike at any given time is low, implying only low uncertainty regarding the output (that is, we were fairly certain that there would be no output spike in the next bin). In this regime, the uncertainty increased with increases in the firing probability. Thus, the entropy of the output spike train increased after synaptic potentiation (which caused an increase in the average output firing rate; top curve in **Fig. 2b**). The conditional entropy was smaller than the output entropy because, given the knowledge of the input spike train, the predictability of the output spike train was improved.

Plastic properties of the synaptic machinery as well as the passive and active cable properties of dendrites[26,31] may affect both the amplitude and the shape of the somatic EPSP[32–33]. Consequently, EPSPs come in many shapes and amplitudes, and it is important to explore the effect of the EPSP shape indices on the SIE. In Fig. 3 (left column), the peak EPSP of the input synapse was held constant whereas its time course changed (left, inset at top). In Fig. 3a, we measured the SIE as a function of the EPSP time-to-peak for four EPSP peak amplitudes (right), leaving all background synapses unchanged. All four curves were rather flat, implying that for the I&F model and the specific input EPSPs simulated here, the SIE is mainly affected by the value of the EPSP peak, rather than by other shape indices of the EPSP (but see below).

In many studies, the efficacy of a synapse is measured with respect to the input charge the synapse generates[25,33–34]. Figure 3b shows the correspondence between synaptic charge and the SIE when the synaptic charge was held constant for all input EPSPs and the SIE was plotted as a function of the EPSP time-to-peak.

a Fixed peak
b Fixed charge

Fig. 3. Effect of EPSP shape indices on the SIE. (**a**) The SIE as a function of the EPSP time-to-peak, with fixed EPSP peak. Four peak values for the input EPSP were considered (peak values at right). Inset at top shows 2 representative EPSPs, both with 2.4 mV peaks and a time-to-peak of 1 ms and 10 ms, respectively (scale bar, 10 ms, 2 mV). EPSPs were simulated by an α-function (see Methods). Arrows at bottom mark the SIE for these representative EPSPs. (**b**) As in (**a**) but the input synapse injected a fixed charge (see Methods). Inset depicts 2 EPSPs, both with input charge of 0.1 nC and a time-to-peak of 1 ms and 10 ms, respectively. (**c, d**) Input EPSP (top frames, same EPSPs as in insets of **a** and **b**) and the corresponding raster plot (middle) and CC (bottom). In the raster plots, for every input spike (aligned at time 0), we plotted the output spikes in the subsequent 30-ms time window. We sorted the plots such that cases with at least 1 output spike in the time window appeared in the lower part. We omitted spikes preceding the input spikes for clarity. The horizontal dashed line shows the number of time windows containing spikes that were expected by chance (computed by randomly sampling the 200-s long-output spike train in 30-ms bins, and multiplying the proportion of windows containing at least 1 spike by the total number of input spikes). The CC (lower frames) was computed between the input spike train and the output spike train (open area), as well as between one background spike train and the output spike train (filled area). A bin size of 1 ms was used. The same I&F model as in Fig. 2 was used.

The two lower panels in Fig. 3c show the CC between the input spike train and the output spike train. The sharp CC corresponded to the brief EPSP, whereas the broad EPSP resulted in a shallower CC covering a larger area. This increase in area corresponds to the increase in the probability for an output spike with an increase in the EPSP area. Both CCs were narrower than the corresponding EPSPs[12].

When the synaptic charge was held constant (**Fig. 3d**), the probability of an output spike, given the input spike, was virtually unaffected by the shape of the EPSP. In fact, the number of output spikes in the 30-ms time window after an input spike was almost identical for both the sharp and the broad EPSPs (978 versus 961, respectively; **Fig. 3d**, middle), and the area of the corresponding CCs was also similar (**Fig. 3d**, bottom). However, the accuracy (time locking) of the output spikes became less precise when the EPSP was broader. The consequence was a decrease of the SIE with broadening of the EPSP, as depicted in Fig. 3b. This decrease in temporal accuracy may have resulted in a marked decrease in the information rate transmitted by the synapse. For example, observing the top curve in Fig. 3b, the SIE for an EPSP with a 1-ms rise time was 18.2 bits s^{-1}, whereas it was only 5.4 bits s^{-1} for an EPSP with a 14.5-ms rise time.

In summary, the EPSP shape affected both the probability of an output and the time locking (temporal accuracy) between the

Although the synaptic charge was fixed, the SIE decreased markedly with increases in the EPSP time-to-peak.

To better understand the results in Fig. 3a and b, Fig. 3c examines the effect of the input synapse with a fixed peak EPSP amplitude once for a brief input EPSP (top left), and once for a broad EPSP (top right), keeping the background activity identical. The raster plot (middle) shows the output spikes in a 30-ms time window after each of the spikes activating the input synapse. In the left raster plot, 655 input spikes (of a total of 1,942) were followed by an output spike within the 30-ms time window. As expected from a sharp EPSP, in most cases the output spike was tightly locked to the input spike (dense vertical region near time 0). For the broader EPSP (right), almost twice (1,095) the number of input spikes were followed by an output spike within the time window. However, the time locking of the output spikes was less precise. These two consequences of EPSP broadening (the increase in probability for an output spike and the decrease in the time locking) affected the SIE in opposite directions, leading to flat curves in Fig. 3a.

Fig. 4. SIE is context dependent. (**a**) Effect of activation frequency of the input synapse on the SIE. Three EPSP peak amplitudes were considered. Background frequency remained fixed at 10 spikes s^{-1}. (**b**) Effect of the frequency of the background excitatory synapses on the SIE. The results for 6 values of peak input EPSPs are shown. To preserve the balance between excitation and inhibition, when the frequency of the background excitatory synapses was increased, G_{max} for the inhibitory synapses was increased proportionally. Neuron model and the background synapses were as in Fig. 2.
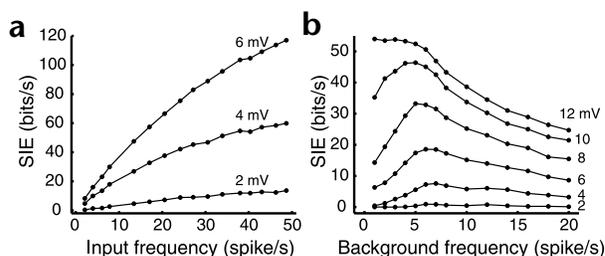
Fig. 5. Effect of dendritic input location on the SIE. (**a**) Model used consisted of a 1-λ-long passive cylindrical dendrite, which was coupled to an isopotential passive soma. An axon with Hodgkin-and-Huxley-like kinetics[21] was connected to the soma. We uniformly distributed 400 excitatory and 100 inhibitory conductance-based synapses over the dendritic cylinder (see Methods). We placed the excitatory input synapse at one of 3 locations (proximal, red; middle, green; distal, blue). (**b**) The SIE as a function of peak synaptic conductance for the 3 input locations depicted in (**a**). Inset shows the resultant soma EPSPs when the input synapse was activated alone. (**c**) Same as in (**b**), but the SIE was plotted as a function of the peak soma EPSP generated by the input synapse. This peak was measured after incorporating the shunt imposed by the background synaptic activity into the dendritic membrane conductance[8,11]. To allow for measurement of suprathreshold EPSPs, active conductances at the axon were set to their value at the resting potential. (**d**) Top, two-soma EPSPs measured in the absence of background activity. The EPSP at left was just at threshold when activated alone (taking into account the average depolarization and conductance change due to background synaptic activity). The EPSP at right was twice the just-threshold EPSP. Middle, 25 randomly chosen superimposed somatic voltage traces that followed the activation of the input EPSPs shown at top. (All EPSPs were aligned at time 0.) Bottom, the corresponding raster plots.
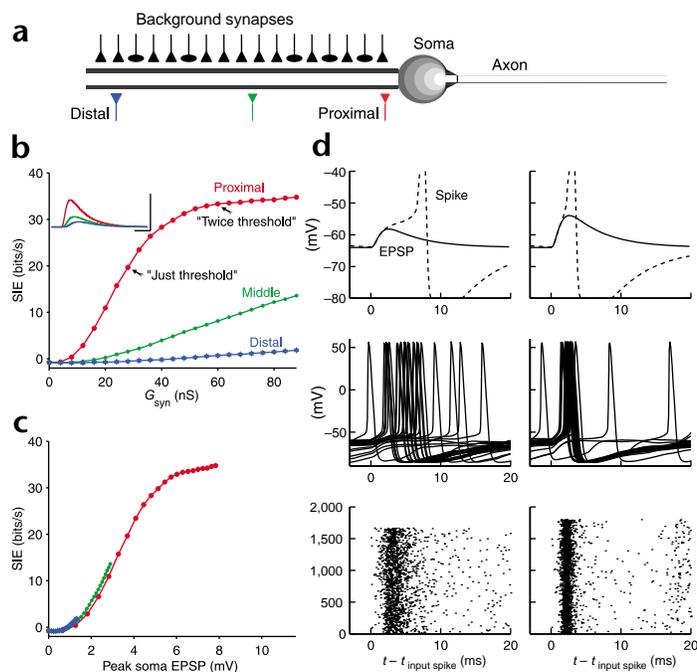
input spike and the output spike. Each of these effects corresponded most closely to one of the factors determining the SIE. The change in the probability of an output spike mainly affected the output entropy, $H(S_{out})$, whereas the accuracy of the output spike, given an input spike, mainly affected the conditional entropy, $H(S_{out}|S_{in})$. Thus, when we kept the synaptic charge fixed while increasing the EPSP rise time, the average rate of output spikes remained almost constant, and thus the output entropy was also fairly constant. The conditional entropy, in contrast, increased with the increase in the EPSP rise time (the uncertain-

ty regarding the time of occurrence of an output spike was larger) and approached the output entropy. Because the SIE is the difference between the output entropy (which remained fairly constant) and the conditional entropy (which increased), the SIE decreased when the EPSP rise time increased (assuming constant synaptic charge).

In contrast, when we kept the EPSP peak constant while increasing its rise time, the synaptic charge increased. This resulted in an increase in the output rate (an increase in $H(S_{out})$), whereas the accuracy of the output spikes, given an input spike, decreased (an increase in $H(S_{out}|S_{in})$). Because both the output entropy and the conditional entropy increased at the same rate when the rise time increased, the SIE remained almost constant for the specific EPSP time course simulated in Fig. 3a. Indeed, for a fixed voltage peak, it is the balance between the EPSP rise time and the EPSP charge that determines SIE. For example, for a fixed EPSP peak value and rise time, an increase in SIE was expected with an increased synaptic charge. This was the case when comparing the left columns in Fig. 3c and d. For these two EPSPs, both amplitude and rise time were almost identical, and only the synaptic charge was larger for the EPSP in the left column of Fig. 3d. Consequently, SIE associated with the broader EPSP was 2 bits s^{-1} and that associated with the brief EPSP was only 0.53 bits s^{-1} (**Fig. 3a** and **b**).
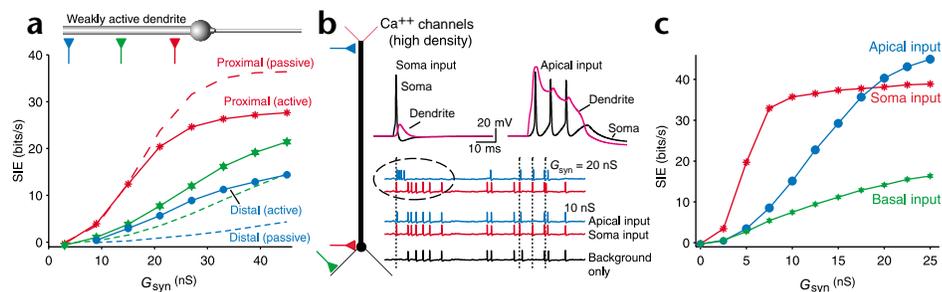
Fig. 6. SIE in nonlinear dendrites. (**a**) Subthreshold nonlinearities. The same model as in Fig. 5 with a low density (1 pS μm^{-2}) of voltage-dependent Na$^+$ ion channels over the dendritic surface. To enhance membrane voltage fluctuations, soma input resistance was slightly increased and the time-to-peak of G_{syn} was decreased to 0.3 nS. The SIE as a function of peak G_{syn} is shown for the proximal, middle and distal input synapses (continuous line for the active case and dashed line for the corresponding passive case). (**b**) Suprathreshold nonlinearities. A simplified model of a pyramidal cell composed of a soma, apical dendrite and 4 tuft and 4 basal dendrites (only 2 of each are shown). Kinetics and spatial distribution of active currents were identical to those in Fig. 1. Density of both voltage-dependent Ca^{++} channels and of Ca^{++}-activated K$^+$ channels was increased in the tufts to 10 pS μm^{-2} and the density of dendritic Na$^+$ channels was reduced to 16 pS μm^{-2}. Sufficiently strong current input at the proximal location induced a single Na$^+$ action potential in the axon, which propagated semi-actively backward into the apical dendrite (top left). Current input to the distal apical dendrite induced a dendritic Ca^{++} spike, which resulted in a burst of Na$^+$ spikes in the axon (top right). At bottom, examples of the somatic action potentials with background synaptic activity when G_{syn} progressively increased. Vertical dashed lines show the activation times of the input synapse. With potentiation of the distal synapse (blue trace at top), bursts of spikes appeared in some cases, and some background spikes disappeared (dashed circle). (**c**) The SIE as a function of G_{syn} for the 3 input synapses depicted in (**b**). With small potentiation, the distal synapse (blue) became more effective than the basal synapse. For larger potentiation, the SIE of the distal input was even larger than that of the proximal synapse.

SIE is context dependent

The SIE depended not only on the properties of the input synapse but also on the statistics of the input and the output spike trains. Changes in either the properties of the background activity (the context) or the characteristics of the input spike train were expected to affect the SIE. In Fig. 4a, the frequency of the spikes activating the input synapse increased whereas the frequency of the background synapses remained fixed. We computed the SIE for the input synapse as a function of the input frequency for three peak EPSP values (denoted at right). All curves increased monotonically with input frequency because more output spikes per unit time were contributed by the input synapse. Increasing the input frequency also increased the input entropy. Normalizing the SIE by the input entropy resulted in an almost constant value of 0.05, 0.3 and 0.6 (unitless) for the cases plotted, respectively. This implies that, for a given EPSP peak and background statistics, the fraction of the information contained in the input that was conveyed by the synapse was almost independent of the input frequency.

In Fig. 4b, we fixed the frequency of the input synapse and increased the frequency of the background synapses. For low background frequencies and a relatively weak input synapse, the probability that the input synapse would trigger an output spike was low and the corresponding SIE was small (lower curves). Membrane voltage fluctuations increased with an increase in background frequency, and this increased the probability that the input synapse would cross threshold for spike firing. Therefore, the SIE increased in this regime (early rising phase). A further increase in the background activity increased the noise (more output spikes resulted from the background activity), and, consequently, the efficacy of the input synapse was reduced. Indeed, for small and intermediate values of the input synapse, the SIE showed a maximum at relatively low background frequencies. These results agreed with results from stochastic resonance theory[35]. In the case of very large input EPSPs (top curve), for which every input spike triggered an output spike in the absence of background activity, the SIE was reduced monotonically with increases in background frequency. SIE may have been affected by temporal correlations within the background activity, depending on whether the input synapse was correlated with the background (not shown).

SIE in dendritic neuron models

The I&F model used thus far ignored the effect of cable properties of dendrites on the integration of synaptic inputs, as well as the effect of the dynamics of the spike generation mechanism in the axon. Because of the passive cable properties of dendrites, the peak of the EPSP severely attenuates and is delayed, and the time course (shape) of the EPSP changes as it spreads from the dendrites to the soma. The farther the input is from the soma, the slower the rise time and the broader the resultant somatic postsynaptic potential[31,34,36–37]. In contrast to the considerable attenuation of the postsynaptic potential's peak, a substantial fraction of the synaptic
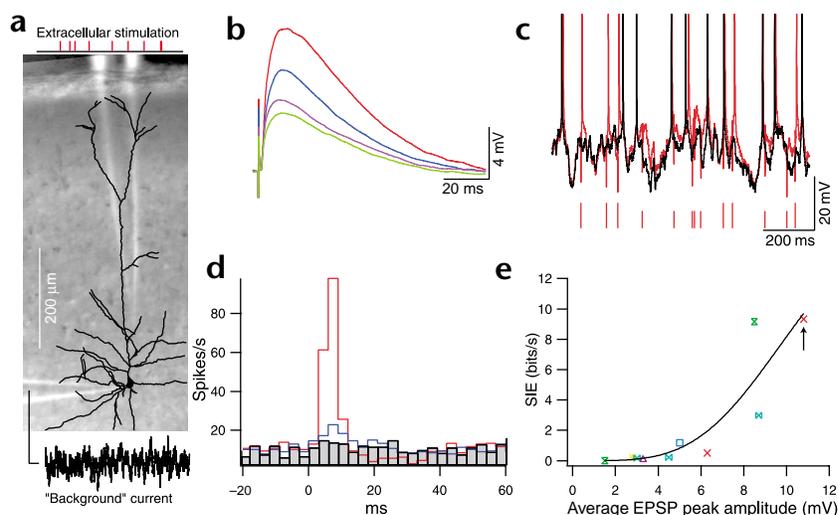
Fig. 7. Experimental measurements of the SIE. (**a**) Layer 5 pyramidal neuron from the somatosensory cortex filled with biocytin and reconstructed in 3D. We used a patch electrode at the soma to inject a fluctuating background current, which mimicked random background synaptic activity (see Methods). We used a second extracellular electrode to stimulate synaptic input. (**b**) Average somatic EPSP recorded in this neuron in response to 4 extracellular stimulus intensities. (**c**) Sample voltage recording (1 s) showing the response to the background current (black trace) and to the strongest extracellular stimulus (red input in **b**) activated together with the background input (red trace). The vertical red ticks show the times of extracellular stimulus activation; the longer ticks depict the cases in which the input EPSP was followed by a time-locked output spike. (**d**) The corresponding cross-correlograms (black, background alone; colors, corresponding inputs in **b** were activated together with the background input). (**e**) The SIE was plotted as a function of the average somatic EPSP amplitude for 6 different cells (each represented by a different symbol and color). A sigmoid function (black line) was used for the fit. The arrow marks the result for the case depicted in red in (**b**–**d**).

charge does reach the soma[37]. Background synaptic activity dramatically increases the membrane conductance of the dendrites, leading to an increase in their electrotonic length and to a decrease in the effective membrane time constant[8–11,38]. Realistic spike mechanisms may introduce complicated subthreshold nonlinearity and history-dependent membrane voltage dynamics. Figure 5 shows the neuron model used, consisting of a passive cylindrical cable (dendrite) coupled to an isopotential soma, which is attached to an excitable axon with a Hodgkin-and-Huxley-like spike mechanism[21]. Excitatory and inhibitory synapses were distributed over the dendritic surface, and each was simulated as a transient conductance change (see **Fig. 5a** and Methods).

In Fig. 5b, we plotted the SIE as a function of the peak synaptic conductance for three dendritic input sites (proximal, middle and distal). The curve for the proximal synapse (red) was qualitatively similar to that found for the I&F model in Fig. 2b, implying that the qualitative behavior of SIE was model independent. The SIE for the middle and distal synapse did not reach saturation even for very large synaptic conductance. This was the direct consequence of the local saturation of the synaptic current at the input site, as well as the severe attenuation of the peak EPSP in the dendrite. As a result, in passive dendrites, distal dendritic synapses were substantially less efficient than proximal synapses.

In the I&F model, the EPSP peak corresponded closely to the SIE, whereas the exact shape of the EPSP had a relatively minor effect (**Fig. 3b**). In Fig. 5c, the same data as in Fig. 5b were plotted against the peak amplitude of the soma EPSP. We measured this peak after rescaling the passive membrane conductance of the cylindrical dendrite to account for the effective change in

dendritic membrane conductance due to the background synaptic activity[8,11]. The three curves overlapped, implying that, as in the I&F model, the relationship between the EPSP peak and the SIE was very similar for all synaptic locations. However, this occurred only when the EPSP peak was rescaled to incorporate the shunting effect of the background synaptic activity. This is yet another aspect of the dependence of the SIE on the context within which the input synapse operates (see Discussion).

The spike generation mechanism affected the SIE in a manner that was not seen in the I&F model (**Fig. 5d**). The top frames show two suprathreshold EPSPs (just-threshold EPSP at left and twice-threshold EPSP at right). Both EPSPs were initiated at a proximal site and almost always generated a spike when activated in the presence of all other background synapses (**Fig. 5d**, middle and bottom). However, the larger EPSP at right generated more accurate (time locked) output spikes. This increase in temporal accuracy of the output spike was mostly due to the shortening of the delay in spike initiation with an increase in the temporal derivative of the input EPSP[12,39]. (Compare dashed curves, a representative spike, in the top frames of **Fig. 5d**.) The two arrows in Fig. 5c indicate the corresponding SIE for these two EPSPs. Although both EPSPs were suprathreshold and yielded approximately the same total number of output spikes, the SIE increased by 15 bits s^{-1} because of the increase in time locking for the larger EPSP.

Effects of dendritic nonlinearities on the SIE

Dendrites are equipped with a variety of voltage-gated ion channels. When activated, these channels may affect the shape and amplitude of the input EPSP, and they may also have a substantial effect on the membrane voltage fluctuations (noise) due to background synaptic activity[10,40]. Figure 6 highlights some effects of excitable dendrites on synaptic information efficacy.

Figure 6a focuses on the effect of dendritic nonlinearities in the subthreshold regime. Voltage-gated Na$^+$ channels at very low density were uniformly distributed over a passive cylindrical dendrite. With a relatively large local excitatory conductance change at distal locations, these ion channels boosted the single EPSP, as measured at the soma, approximately twofold (not shown). For proximal inputs, the amplification due to the excitable dendritic channels was relatively much smaller. (Distal inputs experienced larger local depolarization, and they also had the advantage of being amplified while propagating towards the soma.) The membrane voltage fluctuations due to background synaptic activity as measured at the soma were also boosted by the voltage-gated dendritic ion channels but to a relatively lesser degree as compared with the boosting of individual distal excitatory inputs. The result was an increase in the SIE for distal synapses in the active case as compared with the corresponding passive case (blue curves in **Fig. 6a**). The opposite was true for proximal inputs. In the case of an excitable dendrite, the enhanced noise due to background synaptic activity overwhelmed the (relatively small) amplification of individual proximal inputs. As a consequence, the SIE of the proximal synapses was reduced in the excitable case (red curves) as compared with the passive case. The interactions among dendritic geometry, background synaptic activity, input location and membrane excitability determined whether the efficacy of a given input will increase, decrease or remain unaffected by dendritic excitability.

Figure 6b shows the case of a high density of voltage-gated Ca^{++} channels at distal dendritic tufts. Sufficiently strong individual inputs at proximal sites gave rise to a single Na$^+$ action potential in the axon (top left). This action potential propagated actively backwards (with attenuation) into the dendrites. When this synaptic input was activated at the distal tuft, a large Ca^{++} spike was initiated locally, and this resulted in a burst of Na$^+$ action potentials in the axon (top right)[23]. When background synaptic activity was present (bottom traces), strong distal inputs gave rise to occasional bursts of spikes at the soma (encircled blue trace), which were typically followed by a quiescent period without action potentials. These added spikes in the axon that were followed by a decrease in the background spikes may have resulted in a larger SIE for distal inputs, as compared with corresponding proximal inputs (the blue curve crosses the red curve for large G_{syn} values in **Fig. 6c**). Thus, suprathreshold dendritic nonlinearities may counterbalance the effect of voltage attenuation in dendrites as well as the effect of background noise.

Experimental measurements of SIE

The SIE can also be measured under experimental conditions, where trial-to-trial variability and other noise sources exist (**Fig. 7**). Somatic patch recordings were made from six cortical pyramidal neurons in a slice preparation, and a fluctuating current was injected through this electrode to simulate random background synaptic activity. A test excitatory synaptic input was delivered through extracellular stimulation, and the voltage response of the postsynaptic neuron to the combination of background noise and the synaptic input was measured. Increasing the strength of the extracellular stimulation resulted in EPSP sizes ranging from 2 to 12 mV (**Fig. 7b**). The effect of this input on the output spike train can be seen in the raw traces (**Fig. 7c**) and in the corresponding CC plots (**Fig. 7d**). Because the background voltage fluctuations were large (as required for generating an average spike rate of 10 spikes s^{-1}), a relatively strong synaptic input was required to elicit time-locked spikes.

The summary of the results for the SIE in all six cell recordings is shown in Fig. 7e. The arrow points to the specific case shown in Fig. 7b and c (red trace). Despite the large noise expected when pooling responses from different cells (with different input resistance, different voltage threshold for spike firing and substantial fluctuations in the response to the synaptic stimulus, for example, due to short-term synaptic dynamics), it was possible to measure the SIE reliably. Furthermore, the SIE increased with EPSP size as theoretically expected (**Figs 3–5**). In this set of experiments, the SIE was far from saturation. Indeed, even the largest input EPSP that was used did not always generate an output spike (**Fig. 7c**).

DISCUSSION

Synapses are primarily responsible for transmitting information among nerve cells. It is thus useful to explore the theoretic implications of the electrical and plastic characteristics of synapses for this information transfer. The SIE, the new measure suggested in this study, makes it possible to assess the key factors at the synaptic, dendritic and network levels that govern information transmission by an excitatory synapse. The general theoretical approach used here can easily be extended to explore questions such as: what factors determine the SIE of inhibitory synapses? What is the effect of synaptic dynamics (short-term depression/facilitation), as well as the probabilistic nature of the synapses, on the SIE? What is the effect of the input structure (for example, of bursts of spikes activating the input synapse[41]), as well as the spike generation mechanism in the axon, on the SIE?

The SIE is not a set number for a given synapse, but depends on the properties of the network in which the synapse is embedded (the number, strength and statistics of background synapses—that is, the context). For a given context, one may explore the effect of

specific synaptic or dendritic parameters on the amount of information that the synapse transmits. It is the relative (rather than absolute) values of SIE in the different cases explored that provide the key insights obtained in this study.

The information transmitted by an excitatory synapse increases with the average number of output spikes initiated by the synapse, as well as with the accuracy of time locking between the input synapse and the output spike. Increases in output rate are most sensitive to the total synaptic charge at the soma/axon region, whereas the degree of time locking between input and output is most sensitive to the rate of rise of the somatic EPSP[12,39]. In passive dendrites, for a given peak somatic EPSP, the increase in rise time associated with distal synapses (implying temporally less accurate output spikes) is accompanied by broadening of the EPSP. In terms of the SIE, these two opposite effects tend to cancel each other, making distal and proximal synapses with similar somatic EPSP peaks (measured after incorporating the shunting effect of network activity; **Fig. 5c**) roughly equally effective. This correspondence between the isolated somatic EPSP amplitude and the SIE is no longer valid when voltage-gated dendritic processes are important in determining the voltage dynamics. It would also be erroneous to assume that the isolated peak soma EPSP is a good predictor of the SIE when the background synapses are correlated with the input.

The severe attenuation of the EPSP peak from distal inputs implies a considerable reduction in the SIE in passive trees compared with proximal synapses. It is possible to boost the SIE of distal synapses by increasing the synaptic conductance of distal dendritic synapses[42]. When many such synapses operate simultaneously, however, as is the case *in vivo*, they substantially shunt the dendritic membrane and this reduces the peak soma EPSP from distal synapses considerably more than those for proximal synapses[11]. Alternatively, voltage-gated mechanisms (either at the synapse or at the dendritic membrane) could compensate for the dendritic voltage attenuation[26,33,43–44]. As a consequence, the SIE could become similar (or even larger) for distal compared with proximal synapses. An important message of this study is that any boosting mechanism that enhances individual synaptic input also affects the noise associated with all other background synapses[11,40]. Whether the boosting mechanism increases or decreases the SIE of a given input depends on the ratio between the signal (generated by the input synapse) and the noise (generated by all other synapses).

Finally, the results presented in Fig. 7 indicate that many of the theoretical predictions of this study are experimentally testable. Multiple electrodes allow simultaneous recording from the dendrites and soma of synaptically connected neurons and quantitative computing of the SIE for various input sources, input statistics and input locations[2,6,23–24]. If tightly linked to the theoretical framework presented here, these experiments should shed light on the functional meaning of the synapse. These experiments will provide an opportunity to understand the transformation of the digital character of nervous impulses to an analog postsynaptic potential in the dendrites, which then changes back to a digital signal in the axon of the postsynaptic neuron. The SIE thus captures the information rate that is transmitted by this digital-to-analog-to-digital transformation.

METHODS

Input and output spike trains. We generated random presynaptic spike trains with a specified average rate by sampling an exponential distribution, using the random number generator of Matlab (version 5.3; www.mathworks.com). We omitted intervals <3 ms to account for refractory periods.

Numerical simulations. We carried out numerical simulations using NEURON[45]. Each epoch simulated 200 s. We implemented an I&F spike mechanism using a special module in NEURON that resets the voltage (to $V_{rest} = 65$ mV) after crossing of the firing threshold (–55 mV) for a refractory period of 3 ms. We implemented synaptic inputs using a continuously integrated kinetic scheme. For a linear synapse, the synaptic current was $I_{syn}(t) = G_{syn}(t)(V_{syn} - V_{rest})$, using $G_{syn}(t)$ with a shape of an α-function. If not otherwise stated, the background activity was composed of 400 excitatory synapses ($V_{syn} = 0$ mV, $t_{peak} = 0.5$ ms, $G_{max} = 2$ nS and a mean input frequency of 10 spikes s^{-1}) and 100 inhibitory synapses (75 mV, 0.75 ms, 5 nS, 65 spikes s^{-1}). We preserved a fixed synaptic charge while changing the input time course (**Fig. 3b**) by increasing t_{peak} and decreasing G_{max} proportionally.

We generated EPSPs with a shape of an α-function (**Fig. 3a**) by injecting a current that was computed using the Laplace transform of an α-function, divided by the transform of an RC filter, and taking the inverse Laplace transform. This method is applicable only for single passive RC compartments.

Experiments. We made somatic patch clamp recordings from layer 5 pyramidal cells in slices of somatosensory cortex prepared using standard techniques[24] from P28 Wistar rats and maintained at 32–35°C (for details of extracellular and intracellular solutions, see **Supplementary Methods 2**). To generate background synaptic input, we convolved white noise with an exponential decay with a time constant of 1 ms and adjusted the variance and amplitude to give a spike rate of ~10 spikes s^{-1} with a c.v. of ~1. We alternated sweeps with background current alone (60 s) with sweeps where the identical background current was applied together with synaptic input evoked by extracellular stimulation (using a Poisson train at 10 spikes s^{-1} mean rate). We periodically monitored the amplitude of the synaptic input using a 10 Hz train applied in the absence of background input.

Estimation of the SIE. We estimated the SIE as follows:

$$\text{SIE}(S_{in}; S_{out}) = \hat{H}_n(S_{out}) - \hat{H}_n(S_{out}|S_{in}) \tag{1}$$

where S_{in} and S_{out} are the binned input and output spike trains, respectively, of length n bins. $\hat{H}_n(S_{out})$ is the estimated entropy of the output spike train (see below) and $\hat{H}_n(S_{out} \mid S_{in})$ is the estimated output spike train entropy given the input spike train (the conditional entropy; see **Supplementary Methods 1**).

For illustration, let $S_{out} = (x_1, x_2, ..., x_n)$, where $x_i \in \{0,1\}$ represents the ith bin, and assume that this string is the realization of a stationary and ergodic stochastic process $x = \{x_i\}_{i=1}^{n}$. We can now use the Shannon MacMillan Brieman theorem[46]:

$$-\frac{1}{n}\log_2 p(x_1, x_2, ..., x_n) \xrightarrow[n\to\infty]{} H \tag{2}$$

where H is the entropy rate of **X** and $p(x_1, x_2, ..., x_n)$ is the probability of obtaining the string $(x_1, x_2, ..., x_n)$ as a realization of **X**.
Let $\hat{p}(x_1, x_2, ..., x_n)$ be an estimator of $p(x_1, x_2, ..., x_n)$. We then use the following estimate for the entropy:

$$\hat{H}_n = -\frac{1}{n}\log_2 \hat{p}(x_1, x_2, ..., x_n) \tag{3}$$

The context-tree weighting algorithm proposed by Willems *et al.*[19] provides such an estimator, denoted $p_w^\lambda(x_1, x_2, ..., x_n)$, which is a good estimator under all possible Markov processes with memory bounded by an integer D. This idea can be easily applied for estimating conditional entropies. The depth parameter D assumed by the context-tree weighting algorithm was 10 bins (30 ms) for the simulation of the I&F model and for the experimental data, and 15 bins (45 ms) for the models with realistic spike generation mechanisms. Larger values produced minor differences.

Entropy estimation is vulnerable to undersampling problems[47–49]; a detailed investigation of this issue will be published elsewhere

(Schreibman *et al.*, manuscript in preparation). We note that, in our data, the estimation did not substantially change for spike trains >100 s, whereas for simulations we used spike trains that were 200 s. In the experimental data (in which we used epochs of 60 s), we combined several epochs together in the counts of the weighted context tree (see **Supplementary Methods 1**).

Note: Supplementary Methods are available on the Nature Neuroscience website.

1. Sherrington, C. S. The central nervous system. in *A Text-Book of Physiology* 7th edn. Vol. 3 (ed. Foster, M.) (Macmillan, London, 1897).
2. Tsodyks, M. V. & Markram, H. The neural code between neocortical pyramidal neurons depends on neurotransmitter release probability. *Proc. Natl. Acad. Sci. USA* **94**, 719–723 (1997).
3. Abbott, L. F., Varela, J. A., Sen, K. & Nelson, S. B. Synaptic depression and cortical gain control. *Science* **275**, 220–224 (1997).
4. Manwani, A. & Koch, C. Detecting and estimating signals over noisy and unreliable synapses: information-theoretic analysis. *Neural Comput.* **13**, 1–33 (2001).
5. Fuhrmann, G., Segev, I., Markram, H. & Tsodyks, M. Coding of temporal information by activity-dependent synapses. *J. Neurophysiol.* **87**, 140–148 (2002).
6. Markram, H., Lubke, J., Frotscher, M., & Sakmann, B. Regulation of synaptic efficacy by coincidence of postsynaptic APs and EPSPs. *Science* **275**, 213–215 (1997).
7. Gil, Z., Connors, B. W. & Amitai, Y. Efficacy of thalamocortical and intracortical synaptic connections: quanta, innervation, and reliability. *Neuron* **23**, 385–397 (1999).
8. Bernander, O., Douglas, R. J., Martin, K. A. C. & Koch, C. Synaptic background activity determines spatio-temporal integration in single pyramidal cells. *Proc. Natl. Acad. Sci. USA* **88**, 11569–11573 (1991).
9. Borg-Graham, L. J., Monier, C., & Fregnac, Y. Visual input evokes transient and strong shunting inhibition in visual cortical neurons. *Nature* **393**, 369–373 (1998).
10. Destexhe, A. & Pare, D. Impact of network activity on the integrative properties of neocortical pyramidal neurons *in vivo*. *J. Neurophysiol.* **81**, 1531–1547 (1999).
11. London, M. & Segev, I. Synaptic scaling *in vitro* and *in vivo*. *Nat. Neurosci.* **4**, 853–855 (2001).
12. Fetz, E. E. & Gustafsson, B. Relation between shapes of post-synaptic potentials and changes in firing probability of cat motoneurones. *J. Physiol. (Lond.)*, 387–410 (1983).
13. Abeles, M. *Corticonics*. (Cambridge Univ. Press, Cambridge, 1991).
14. Hebb, D. O. *The Organization of Behavior* (Wiley, New York, 1949).
15. Hoppfield, J. J. Neural networks and physical systems with emergent collective computational abilities. *Proc. Natl. Acad. Sci. USA* **79**, 2254–2258 (1982).
16. Yamada, S., Nakashima, M., Matsumoto, K. & Shiono, S. Information theoretic analysis of action potential trains. I. Analysis of correlation between two neurons. *Biol. Cybern.* **68**, 215–220 (1993).
17. Rieke, F., Warland, D., de Ruyter van Steveninck, R. & Bialek, W. *Spikes: Exploring the Neural Code*. (MIT Press, Cambridge, Massachusetts, 1997).
18. Borst, A. & Theunissen, F. E. Information theory and neural coding. *Nat. Neurosci.* **2**, 947–957 (1999).
19. Willems, F. M. J., Shtarkov, Y. M. & Tjalkens, T. The context-tree weighting method: basic properties. *IEEE Trans. Info. Theory* Vol. IT-41, 653–664 (1995).
20. Pinsky, P. F. & Rinzel, J. Intrinsic and network rhythmogenesis in a reduced traub model for ca3 neurons *J. Comput. Neurosci.* **1**, 39–60 (1994) [erratum in *J. Comput. Neurosci.* **2**, 275 (1995)].

21. Mainen, Z. F. & Sejnowski, T. J. Influence of dendritic structure on firing pattern in model neocortical neurons. *Nature* **382**, 363–366 (1996).
22. Segev, I. & London, M. Untangling dendrites with quantitative models. *Science* **290**, 744–750 (2000).
23. Larkum, M. E., Zhu, J. J. & Sakmann, B. A new cellular mechanism for coupling inputs arriving at different cortical layers. *Nature* **398**, 338–341 (1999).
24. Stuart, G. J. & Häusser, M. Dendritic coincidence detection of EPSPs and action potentials. *Nat. Neurosci.* **4**, 63–71 (2001).
25. Stratford, R. D., Mason, A. J. R., Larkman, A. U., Major, G. & Jack, J. J. B. The modeling of pyramidal neurons in the visual cortex. in *The Computing Neuron* (eds. Durbin, R., Miall, C. & Mitchson, C.) Addison-Wesley, Reading, Massachusetts, 1989).
26. Nicoll, A., Larkman, A. & Blakemore, C. Modulation of EPSP shape and efficacy by intrinsic membrane conductances in rat neocortical pyramidal neurons *in vitro*. *J. Physiol. (Lond.)* **468**, 693–710 (1993).
27. Carnevale, N. T. & Johnston, D. Electrophysiological characterization of remote chemical synapses. *J. Neurophysiol.* **47**, 606–621 (1982).
28. Oertel, D. Synaptic responses and electrical properties of cells in brain slices of the mouse anteroventral cochlear nucleus. *J. Neurosci.* **3**, 2043–2053 (1983).
29. Bernander, O. & Koch, C. The effect of synchronized inputs at the single neuron level. *Neural Comput.* **6**, 622–641 (1994).
30. Murthy, V. N. & Fetz, E. E. Effects of input synchrony on the firing rate of a three-conductance cortical neuron model. *Neural Comput.* **6**, 1111–1126 (1994).
31. Rall, W. Distinguishing theoretical synaptic potentials computed for different soma-dendritic distributions of synaptic input. *J. Neurophysiol.* **30**, 1138–1168 (1967).
32. Liao, D., Hessler, N. A. & Malinow, R. Activation of postsynaptically silent synapses during pairing-induced LTP in CA1 region of hippocampal slice. *Nature* **375**, 400–404 (1995).
33. Cook, E. P. & Johnston, D. Voltage-dependent properties of dendrites that eliminate location-dependent variability of synaptic input. *J. Neurophysiol.* **81**, 535–543 (1999).
34. Iansek, R. & Redman, S. J. The amplitude, time course and charge of unitary excitatory post-synaptic potentials evoked in spinal motoneurone dendrites. *J. Physiol. (Lond.)* **234**, 665–688 (1973).
35. Levin, J. E. & Miller, J. P. Stochastic resonance enhances neural encoding of broadband stimuli in the cricket cercal sensory system. *Nature* **380**, 165–168 (1996).
36. Rall, W. Theoretical significance of dendritic trees for neuronal input-output relations. in *Neural Theory and Modeling* (ed. Reiss, R.) 73–97 (Stanford Univ. Press, Stanford, 1964).
37. Rinzel, J. & Rall, W. Transient response in a dendritic neuron model for current injected at one branch. *Biophys. J.* **14**, 759–790 (1974).
38. Häusser, M. & Clark, B. A. Tonic synaptic inhibition modulates neuronal output pattern and spatiotemporal synaptic integration. *Neuron* **19**, 665–678 (1997).
39. Fricker, D. & Miles, R. EPSP amplification and the precision of spike timing in hippocampal neurons. *Neuron* **28**, 559–569 (2001).
40. De Schutter, E. Dendritic voltage and calcium-gated channels amplify the variability of postsynaptic responses in a Purkinje cell model. *J. Neurophysiol.* **80**, 504–519 (1998).
41. Reinagel, P., Godwin, D., Sherman, S. M. & Koch, C. Encoding of visual information by LGN bursts. *J. Neurophysiol.* **81**, 2558–2569 (1999).
42. Magee, J. C. & Cook, E. P. Somatic EPSP amplitude is independent of synapse location in hippocampal pyramidal neurons. *Nat. Neurosci.* **3**, 895–903 (2000).
43. Reyes, A. Influence of dendritic conductances on the input-output properties of neurons. *Annu. Rev. Neurosci.* **24**, 653–675 (2001).
44. Magee, J. C. Dendritic lh normalizes temporal summation in hippocampal CA1 neurons. *Nat. Neurosci.* **2**, 508–514 (1999).
45. Hines, M. L. & Carnevale, N. T. The NEURON simulation environment. *Neural Comput.* **9**, 1179–1209 (1997).
46. Cover, T. M. & Thomas, J. A. *Elements of Information Theory* (Wiley, New York, 1991).
47. Treves, A. & Panzeri, S. The upward bias in measures of information derived from limited data samples. *Neural Comput.* **7**, 399–407 (1995).
48. Strong, S. P., Koberle, R., de Ruyter van Steveninck, R. & Bialek, W. Entropy and information in neuronal spike trains. *Phys. Rev. Lett.* **80**, 197–201 (1997).
49. Schultz, S. R. & Panzeri, S. Temporal correlations and neural spike train entropy. *Phys. Rev. Lett.* **86**, 5823–5826 (2001).
50. Contreras, D., Destexhe, A. & Steriade, M. Intracellular and computational characterization of the intracortical inhibitory control of synchronized thalamic inputs *in vivo*. *J. Neurophysiol.* **78**, 335–350 (1997).